View metadata, citation and similar papers at core.ac.uk
brought to you by CORE
provided by NASA Technical Reports Server

NASA TECHNICAL MEMORANDUM

NASA TM X- 68013

NASA TM X- 68013

CASE FILE COPY

DESIGN, FABRICATION, AND OPERATION OF DISHED ACCELERATOR GRIDS ON A 30-CM ION THRUSTER

by V. K. Rawlin, B. A. Banks, and D. C. Byers
Lewis Research Center
Cleveland, Ohio

TECHNICAL PAPER proposed for presentation at
Ninth Electric Propulsion Conference sponsored by the
American Institute of Aeronautics and Astronautics
Washington, D.C., April 17-19, 1972

DESIGN, FABRICATION, AND OPERATION OF DISHED ACCELERATOR GRIDS ON A 30-CM ION THRUSTER

V. K. Rawlin, B. A. Banks, and D. C. Byers
National Aeronautics and Space Administration
Lewis Research Center
Cleveland, Ohio

Abstract

Several closely-spaced dished accelerator grid systems have been fabricated and tested on a 30-cm diameter mercury bombardment thruster and they appear to be a solution to the stringent requirements imposed by the near-term, high-thrust, low specific impulse electric propulsion missions. The grids were simultaneously hydroformed and then simultaneously stress relieved. The ion extraction capability and discharge chamber performance were studied as the total accelerating voltage, the ratio of net-to-total voltage, grid spacing, and dish direction were varied.

Introduction

E-6796

The electron-bombardment ion thruster is being considered for a variety of space missions for which the optimum specific impulse is between 2000 and 3000 seconds.[1,2] Such values of specific impulse have been obtained with thrusters using composite grids.[3,4,5,6] However, recent data indicate that satisfactory operation of composite grids is dependent on backsputtered facility material.[6] For this reason, it is probable that conventional two-grid accelerator systems will be required for near term missions. Achievement of specific impulses of 2000 to 3000 seconds with two-grid systems at the desired thrust densities and thruster efficiencies requires essentially the following:

(1) The screen grid be less than 0.5 mm thick

(2) The screen grid have a high open area fraction, preferably in excess of 0.7

(3) A grid-to-grid spacing of about 0.25 to 0.75 mm be maintained over the entire grid system

Any practical ion extraction system must also survive both the launch environment and repeated thermal cycling. These factors combine to impose a difficult mechanical design problem. Techniques such as holding the grids in tension, supporting the screen grid from the mercury vapor distributor manifold, adding stiffener ribs, and interelectrode supports have been tested and/or proposed to solve the design problem.[5,7] This paper presents the experimental results concerning the fabrication and operation of dished grids on a 30-cm diameter ion thruster.

Calculations are also made concerning the deflection of dished grids under thermal loading and thrust losses arising from the spherical shape of the grids. SI Units are used throughout, and the symbols are defined in the Appendix.

Apparatus and Procedure

Dished Grid Fabrication

The grid-to-grid spacing determines the electrical breakdown strength and, combined with the hole diameter, determines the ion beamlet focusing characteristics and ion beam current extraction capability. A rule of thumb which previously has been used in the design of ion thrusters is that the aspect ratio or unsupported span to grid spacing ratio be in the range of 50 to 70 avoid problems during operation.[8]

Aspect ratios of 400 to 1200 are necessary for a 30-cm thruster without grid supports to satisfy the requirements imposed by near term missions listed in the Introduction.

To obtain a uniform small grid spacing (0.25 to 0.75 mm) over a 30-cm diameter requires that the contours of the adjacent surfaces of the screen and accelerator grids be nearly identical. That is to say, any local irregularities (bumps, wrinkles, etc.) must occur at the same location and to the same degree in both grids. Fabrication techniques which dish both grids simultaneously tend to minimize grid spacing variations. Numerous techniques have been employed in attempts to fabricate dished accelerator grid systems. These include spinning, hot and cold pressing, and hammering. However, irregularities in the resulting grid contours were so severe that the grids could not be successfully used as a closely spaced grid system.

Simultaneous hydroforming of dished grid systems has recently produced well-matched molybdenum 30-cm grids with grid spacing variations of less than 0.1 mm. The screen and accelerator grids to be dished by this technique are first riveted together around their outer perimeter to insure proper hole alinement. They are then placed over a rubber sheet as shown in Fig. 1. The grids and rubber sheet are tightly clamped between a female die and a base plate. Hydraulic fluid is then pumped in through the base plate to inflate the rubber sheet forcing the grids to take the shape of the female die. All the dished grids tested and reported in this paper were fabricated by this technique. The clamping force was produced by the expansion of aluminum cylinders which were chilled with liquid nitrogen and then (after tightening the nuts) heated up to expand and force the die and base plate together. Figure 2 shows the model and nomenclature chosen to represent a dished grid. All symbols are defined in the Appendix. The resulting grids had a dish depth, h', of approximately 2.23 cm for a diameter, $2R_t'$, of 33.8 cm. The grids were stress relieved by placing them both between matching male and female (same one used in hydroforming) dies which were bolted together and heated in an inert atmosphere. The temperature of the dies was slowly increased in 980 C, held there for 1 hour, and then

slowly cooled to room temperature. The dish depth increased to 2.54 cm during the stress relieving process.

The three grid sets reported in this paper were fabricated at the Lewis Research Center from a 0.38 mm thick arc cast sheet of perforated molybdenum. The grid holes were produced in a hexagonal array over the entire molybdenum sheet by photochemical etching which resulted in the geometries given in Table I. An etch of 50-50 means that the hole was etched 50 percent through from each side of the molybdenum sheet, whereas 90-10 etch means that 90 percent of the hole was etched from one side of the sheet. A sketch of the cross section of the web remaining between the holes is shown in Table I. Cusps were formed because the grid was etched from both sides of the molybdenum sheet. The minimum hole diameter was at the cusp and the maximum was at the grid surface. Equivalent percent open areas were calculated using the minimum and maximum hole diameters. The minimum hole diameters were 1.9 mm for grid sets A and B and 1.2 mm for set C.

Preliminary tests of these grids of Table I were made using insulating spacers of synthetic mica or glass prior to mounting the grids on molybdenum rings. The grid mounting system used for final testing is shown in Fig. 3. Figure 4 shows the grids and mounting system on the thruster with the thruster ground screen removed. The grid set in Fig. 4 was mounted concave when viewed from downstream of the thruster. This dish direction of the grids will be referred to as "concave" throughout the paper. When reversed, the grids will be referred to as "convex"--as viewed from downstream of the thruster.

Thruster and Facility

A 30-cm diameter thruster, previously optimized for use with composite grids, was used to evaluate the dished two-grid accelerator systems. The thruster was built by Hughes Research Laboratories (HRL) under contract NAS3-11523[5] and was used to obtain all of the data presented herein. The HRL thruster was operated in the 3.0 m diameter port of the 7.6 m diameter by 21.4 m long vacuum tank at the Lewis Research Center.[9] The bell jar pressure during thruster operation was about 3×10^{-6} torr while the main tank pressure was 2×10^{-7} torr.

Accelerator Grid Evaluation

Minimum total voltage. - Data such as shown in Fig. 5 were taken to determine the minimum total voltage between the grids at a given beam current which would not lead to accelerator impingement currents greater than 2 to 3 percent of the beam current. This method, which was similar to that used by Kerslake,[8,10] was used consistently to evaluate each grid set relative to other grid sets. At a given beam current and typical operating point, the total accelerating voltage was lowered at a constant ratio of net accelerating voltage (anode voltage) to total accelerating voltage, R. The mercury flow from the main vaporizer was held fixed. The beam current extracted by the grids was also maintained constant by changing the discharge current as required. The discharge voltage was maintained at 40 volts by making small changes in the cathode propellant flow rate. The accelerator impingement current increased rapidly when the total voltage was too low to focus the ions into the accelerator grid holes. Figure 5 shows how the ratio of impingement current to beam current varied with total voltage for several values of beam current. The minimum total voltage was arbitrarily determined as the point where a tangent to each curve had a slope of minus one (0.02/kV).

Electron backstreaming. - Each grid set was checked, at various levels of beam current and net accelerating voltage, for the value of accelerator grid voltage at which electron backstreaming occurred. Electron backstreaming consists of electron flows into the screen grid or discharge chamber from the neutralized downstream beam plasma when the magnitude of the negative accelerator grid voltage was decreased below certain levels which were dependent on operating conditions.

Grid-to-grid spacing measurement. - Two methods of setting or measuring the spacing between the grids were used. "L" shaped wires of various diameters were inserted into the grid holes to determine the grid-to-grid spacing before and after a test. The grid spacings were also measured by intruding a dental impression material into the grid holes and between the grids. After the dental material cured, the grids were separated, the spacing impression was removed, and a photomicrograph was taken. This method has previously been used to measure hollow cathode orifices.[4,5] The cold gird-to-grid spacings measurements are estimated to be accurate within 0.05 mm.

Discharage Chamber Performance

Energy per beam ion versus utilization. - Two methods of obtaining the variation of the energy per beam ion, E_I, as a function of propellant utilization efficiency, η_u, have been used. The first method used a slow point-by-point measurement of η_u in which the beam current and discharge voltage were held fixed. The discharge current and flow rates were varied to produce the curve. The second and faster method required a η_u measurement at a nominal operating point. Then, while the vaporizer heater powers were held constant, the discharge voltage and current were changed to vary the beam current, thereby changing the E_I and η_u. The two methods yielded different curves because the beam current was constant in one case and not in the other. In the second case, the discharge voltage may have increased to a value at which the degree of doubly ionized mercury atoms was not negligible. Also, the temperatures of the mercury vaporizers could have changed due to thermal feedback from the discharge chamber.

Mercury flow rate measurements. - The mercury flow rates were obtained by measuring a drop in the height of a mercury column inside of a calibrated flow tube during a known time interval. Mercury flow rates were repeatable to 1 percent and were estimated to be accurate within 2 percent.

Theoretical Analysis

Grid Deflection

A brief calculation was made of the deflection of dished grids under thermal loading. Because data presented herein were obtained with grids

without intermediate grid supports, the analysis of deflection will be for grids supported only on the edges. It was assumed that the shapes of the screen and accelerator grids were spherical before operation. It was assumed that the radii of curvature of both grids were equal. Figure 2 shows the model used for the calculations.

Present tests indicate that during operation the center of the screen grid heats up to between 350 to 550 C and the center of the accelerator grid to a somewhat lower temperature. Thermal gradients of 350 C could exist between the center of the grids and the ring support. Because the supports are cooler than the grids, the grids deflect by an amount, $\Delta\ell$, which depends on the average temperature of the grid and the temperature of the ring support. It was assumed that the new shapes, shown by the dotted line on Fig. 2, were also spherical. The screen grid was the hotter of the two grids and underwent the most deflection.

The intent of the following calculation is to determine the grid-to-grid spacing variation for various geometries and operating conditions. The variation of spacing is defined as the net difference between the deflection of each grid during operation. Figure 4 shows the grids dished concave, and in this case the grid-to-grid spacing increased during operation. When the grids were dished convex the grids became closer together under thermal loading.

From Fig. 2 it can be seen that the deflection of a single grid, $\Delta\ell$, can be obtained from the equation:

$$\frac{R'_g + \Delta\ell}{\sin\gamma} = \frac{\Delta z}{\sin\beta} \tag{1}$$

The known dimensions are the dish depth, h', and a half chord length, R'_r. The grid has a radius of curvature, R'_g, given by:

$$R'_g = \frac{R'^2_r + h'^2}{2h'} \tag{2}$$

The maximum angle of dish γ'_{max} and the initial arc length of the grid S' are:

$$\gamma'_{max} = \sin^{-1}\left(\frac{R'_r}{R'_g}\right) \tag{3}$$

$$S' = 2\gamma'_{max}R'_g \tag{4}$$

When the grid and grid mounting ring heat up, both expand and the dished area assumes a new half chord length and arc length which are given by:

$$R_r = R'_r(1 + \alpha_r\Delta T_r) \tag{5}$$

$$S = S'(1 + \alpha_g\Delta T_g) \tag{6}$$

where α_r and α_g are the coefficients of expansion of the mounting ring and grid material, respectively. The temperature increases of the ring and grid are ΔT_r and ΔT_g and are both average values. Average temperature values are used to give expansions as if the entire ring or grid were at the average temperatures.

It can be shown to a good approximation that the new values of maximum angle of dish γ_{max} and radius of curvature R_g are:

$$\gamma_{max} = \left[6\left(1 - \frac{2R_r}{S}\right)\right]^{1/2} \tag{7}$$

$$R_g = \frac{R_r}{\sin\gamma_{max}} \tag{8}$$

The maximum value of the angle β is:

$$\beta_{max} = \gamma_{max} - \left(\gamma'_{max} + \Delta\gamma'_{max}\right) \tag{9}$$

where

$$\Delta\gamma'_{max} \cong \frac{R'_r\alpha_r\Delta T_r \cos\gamma'_{max}}{R'_g} \tag{10}$$

The axial distance between the centers of curvature of the grid before and during operation is:

$$\Delta z = \frac{R_g \sin\beta_{max}}{\sin\left(\gamma'_{max} + \Delta\gamma'_{max}\right)} \tag{11}$$

In general

$$\sin\beta = \frac{\Delta z \sin\gamma'}{R_g} \tag{12}$$

and

$$\sin\gamma = \frac{r}{R_g} \tag{13}$$

Substitution of Eqs. (2), (11), (12), and (13) into Eq. (1) gives the deflection of the grid during operation, $\Delta\ell$, at any point P. $\Delta\ell$ is measured along an extension of the initial radius of curvature to P. Equation (1) can be used to determine the deflection of a particular grid configuration. The grid-to-grid spacing variation can be calculated by substituting values of ΔT_r and ΔT_g for both the screen and accelerator into Eq. (5) and (6). Substitution of various values of h' into Eq. (2) can show the effect of various values of dish depth. The results of this calculation are presented later.

Thrust losses from hole misalinement. - The present technique of dishing grids with identical hole patterns leads to a grid hole misalinement which is a function of γ. Figure 6(a) is a section view of the grids after dishing and stress relieving. Figure 6(b) shows the same set of grids during operation with the grids mounted convex. Figure 6(b) also shows that there is a grid hole misalinement (maximum at the outer holes) caused by the grid-to-grid spacing separation.

The current density extracted at the screen grid at element dA and at an angle γ from the thruster axis is defined as $j(\gamma)$. Each beamlet is deflected by γ due to the shape of the grid.

The grid hole misalinement leads to an additional beam deflection, λ, which is a function of γ. The following section will present calculations to determine the effect of dishing on the thrust to beam power ratio. This is a measure of the thrust loss due to ion beam divergence from the grid set as assembled. It is beyond the scope of this report to determine analytically beam deflections due to grid distortions during operation. Such additional beam deflections may add or subtract to the thrust losses caused by the basic grid geometry.

The total axial thrust and beam power of a dished grid can be calculated by:

$$T = \frac{R_g^2 m v}{q} \int_0^{2\pi} d\theta \int_0^{\overline{\gamma}} j(\gamma) \cos(\gamma + \lambda) \sin\gamma d\gamma \tag{14}$$

$$P_B = \frac{R_g^2 m v^2}{2q} \int_0^{2\pi} d\theta \int_0^{\overline{\gamma}} j(\gamma) \sin\gamma d\gamma \tag{15}$$

From Ref. 11, it is shown to a good approximation over a large range of grid designs that

$$\lambda \approx C_1 \frac{\ell}{D_s} \sin\gamma \tag{16}$$

Equations (14), (15), and (16) can be used to calculate the thrust to beam power ratios of dished grids. Two different forms of $j(\gamma)$ were assumed. For the first calculation it was assumed that $j(\gamma)$ was constant. Then it was assumed that

$$j(\gamma) = j(o) \cos\left[\gamma\left(\frac{(\pi)}{2\overline{\gamma}}\right)\right] \tag{17}$$

The authors believe that the actual variation of $j(\gamma)$ is between these two expressions. In the argument of the cosine in Eq. (14), the small angle approximation was made, i.e.,

$$\lambda \approx C_2 \gamma \tag{18}$$

Substitution of Eq. (18) and the two values of ion current density into Eqs. (14) and (15) allows the thrust to beam power ratios to be evaluated in closed integral form.

The value of the thrust to beam power ratio for an ideal grid with no divergence loss is:

$$(T/P)_{ideal} = 2/v \tag{19}$$

To normalize the divergence thrust loss, the values of thrust to beam power ratios calculated from Eqs. (14) and (15) are multiplied by the product $v/2$.

Results and Discussion

Operation of Dished Two-Grid Accelerator Systems

Dished grids have been fabricated and operated on a 30-cm thruster over a large range of test conditions. The grid voltages, spacings, dish direction, and hole diameters have been varied and found to affect the thruster performance. An attempt will be made to separate and discuss these parameters and their effects.

Some geometric properties of the grid sets tested are listed in Table II. Grids with minimum hole diameters of 1.2 and 1.9 mm were tested. The cold (room temperature) grid-to-grid spacing was varied from 0.30 mm to 0.86 mm. The grids were operated convex and concave.

Perveance of dished grids. - The following form of Child's law was used by Kerslake to calculate ion beam currents extracted by the grid systems of ion engines.[8,10]

$$J_B = \frac{8}{9}\epsilon_o \sqrt{\frac{q}{2m}} \frac{A_o}{\ell_g^2} (\Delta V)^{3/2} = 0.386\times10^{-8} \frac{A_o}{\ell_g^2} (\Delta V)^{3/2} \tag{20}$$

For a constant diode configuration, the factors preceding $(\Delta V)^{3/2}$ have been given the name "perveance." The grid sets of Table II were evaluated by determining the minimum acceptable total accelerating voltage at several beam currents as described in the Apparatus and Procedure section. Figure 7 is a plot of the knee voltages at the corresponding beam currents for the six grid sets tested. The shaded portion of Fig. 7 shows the region of composite grid operation from Refs. (4) and (5).

Because all of the dished grids had approximately the same effective open area, the primary cause for the different positions was the different ion accelerating distance of each grid set.

Figure 7 shows that the beam current extracted by each grid set increased with voltage but at a power greater than the three-halves predicted by Child's law. This could occur if the plasma density profile varied as the thruster conditions were changed at higher beam currents. The actual beam currents shown in Fig. 7 are only 20 to 60 percent of the ideal beam current predicted by Eq. (20) when the sum of the hot grid spacing and the screen grid thickness is used for the ion acceleration distance. The experimental perveance is probably less than ideal because:

(1) The plasma density profile is not uniform across the grid.

(2) At the grid spacing to hole diameter ratios used herein, the grid aperture effect[8] predicts reductions of the ideal beam current between 35 and 55 percent.

The data presented in Fig. 7 show that a thruster with dished grid meets the performance requirements of near term, high thrust, low specific impulse missions.

Grid-to-grid spacing. - The perveance for the grid sets of tests 2 and 4 are shown in Table II and Fig. 7. For test 2 the grids were mounted convex and the cold grid spacing was 0.86 mm. For test 4 the grids were mounted concave with a spacing of 0.33 mm. When operated, the perveance of grids of test 2 was identical to that of test 4.

As explained earlier, the spacing of the grids during operation decreased for test 2 and increased for test 4. The change in spacing during operation for the grids of tests 2 and 4 was estimated by assuming that:

(1) Two sets of grids having the same extraction hole geometry and perveance must also have the same effective ion accelerating distance.

(2) Under identical thermal loading, the grid deflection is independent of the grid dish direction.

The change in spacing was expected to be about one-half the difference of the cold spacing, or 0.26 mm. This gave a hot grid-to-grid spacing of 0.60 mm for each test.

Figure 8 is a plot of the beam currents from Fig. 7 at a constant total voltage of 1000 volts as a function of ℓ, the ion accelerating distance. The ion accelerating distance was calculated as the sum of the cold spacing, the 0.38 mm screen grid thickness, and the positive or negative 0.26 mm estimated change in spacing during operation.

Figure 8 shows that the beam current increased as ℓ was decreased. The slope of the line drawn through the data for the grids was 1.9 mm diameter holes is -1.3 rather than -2 as expected from Eq. (20). Again, probable reasons for the reduced experimental beam currents are the nonuniform plasma density profile and the grid aperture effect.

In test 2 the discharge power was varied from 200 to 500 watts at a beam current of 1.0 amperes. The knee value of total voltage was not changed by this variation of thermal loading.

The grid temperature was probably proportional to the fourth root of the discharge power. If this was the case, the spacing probably did not change much during operation and most of the change in grid spacing probably occurred when the discharge was first turned on. Figure 9 shows the calculated variation of grid-to-grid spacing of a grid set during operation for several values of dish depth and an initial value of R'_t of 15 cm. The temperature increases, ΔT_{rS} and ΔT_{rA}, of the screen and accelerator mounting rings were assumed equal to 170 C. The average temperature increase, from room temperature, of the screen grid, ΔT_{gS}, was assumed to be 400 C, and the average temperature increase of the accelerator grid, ΔT_{gA}, was assumed to be 300 C.

The grid-to-grid spacing variation is maximum at the center of the grid and falls to zero at the edge of the grid system. For the conditions assumed for Fig. 9, the maximum change in spacing for a 2.54 cm dish, which was used for all performance data presented herein, was about 0.36 mm. When an average temperature increase of 350 C (instead of 300 C) for the accelerator grid was assumed, the maximum variation in grid-to-grid spacing was 0.18 mm. The 0.36 and 0.18 mm maximum variations in the calculated grid-to-grid spacing are in approximate agreement with the 0.26 mm average variation estimate obtained from the grid operation.

The change in spacing is a strong function of the initial dish depth. For example, the calculated value of the maximum change in spacing decreased by about a factor of 2.5 as the chosen initial dish depth increased from 1.27 to 3.81 cm.

The data of Fig. 9 indicate that to minimize the grid-to-grid spacing variation during operation, it is desirable to fabricate the grids with as deep a dish as possible. On the other hand, the thrust losses increase as the dish depth increases. This thrust loss will be discussed later in the text.

Ratio of net-to-total voltage. - At a fixed total voltage and beam current, the specific impulse of the thruster can be varied, within limits, by changing the ratio of the net-to-total voltage, R.

Figure 10 is a plot of the ratio of the accelerator impingement current to the beam current, as a function of the total voltage at four values of R, for the grid set of test 2. It shows that the knee voltage changed only 90 volts for a variation of R from 0.67 to 0.40. At the lowest value of R, 0.33, the knee voltage became more difficult to determine.

A noticeable effect of R variation is that the base level accelerator impingement current increased with decreasing R. This is also shown in Fig. 11, which is a plot of the ratio of impingement current to beam current for the grids of test 2 as a function of R. The beam current was varied from 1.5 to 2.5 amperes and the total voltage was varied from 1300 to 1700 volts. The propellant utilization efficiency was greater than 0.85 and the total voltage was always greater than the knee value. In general, the ratio of impingement current to beam current increased as R decreased, thereby increasing the accelerator power loss and decreasing the expected accelerator grid lifetime. The data were grouped in a single band showing a primary dependence on only R and not beam current or total voltage. The increase in accelerator current as R was decreased could have been due to either an increase in the amount of direct impingement or an increase in the charge exchange current. The distance for charge exchange to occur increases as R is decreased.[13] Attempts to operate the grids at values of R greater than about 0.75 resulted in an accelerator voltage which was too small in magnitude to prevent electron backstreaming. At R ratios less than 0.5 the ion impingement increased above 1.0 percent of the beam current. This sensitivity of impingement current to R variation for dished grids may be a result of the grid hole misalinement obtained during the dishing process. This problem might be minimized if the grids were dished such that no hole misalinement occurred on the grids.

Grid hole diameter and etch. - Grids with hole diameters of 1.2 and 1.9 mm were tested. The fraction open area of all grids tested was about 0.50. Preliminary results, shown in Figs. 7 and 8, have indicated a loss in the grid extraction capability when the hole size was decreased from 1.9 to 1.2 mm for a constant spacing. Further testing would be required to determine the optimum hole diameter for closely spaced 30-cm diameter grids.

In order to determine the effect, if any, of the grid etch on grid perveance, tests 2 and 5 were conducted. In test 2, both grids had a 50-50 etch while in test 5, the screen grid had a 90-10 etch and the accelerator had a 50-50 etch. The grids of tests 2 and 5 had equal cold spacings of 0.86 mm and were dished convex. As shown in Fig. 8 and Table II, the perveance was identical for both grid sets.

Electron backstreaming. - During the operation of dished grids, the electron backstreaming limit of

the accelerator voltage was found to be a function of the beam current, accelerator grid hole diameter, net accelerating voltage, R, and grid spacing. Figure 12 shows the effect of the value of beam current and the accelerator grid hole diameter on the electron backstreaming limit. The absolute value of the accelerator voltage backstreaming limit increases approximately linearly with beam current. The scatter in the data for grids with 1.9 mm diameter holes is largely due to the wide range of net accelerating voltages used--from 300 to 1200 volts. The backstreaming limit for the grids with 1.2 mm diameter holes was roughly 40 percent of that required for the larger 1.9 mm holes.

The Effects of Dished Grids on Discharge Chamber Performance

References 3, 4, 5, 13, and 14 have shown that the ion extraction system affects the thruster discharge chamber performance. This section presents similar results showing the effect of grid system parameters such as grid type, voltages, and dish direction on the discharge chamber performance.

Grid type. - Figure 13 is a plot of the discharge energy per beam ion, E_I, as a function of the propellant utilization efficiency, η_u, for 30-cm thrusters with several different accelerator grid systems. The E_I of the thruster with the present dished grids was about 325 at a η_u of 90 percent whereas the E_I with composite grids was about 170.[4,5] This increase in E_I was probably due to the decrease in the fraction open area of the dished grids (51 percent) from the effective value for composite grids (estimated to be >90 percent[4]). The thruster on which the dished grids were tested was also optimized for composite grids and it is possible that some improvement in E_I could have been realized with appropriate discharge chamber modifications.

Total voltage. - In general, as the total accelerating voltage was lowered, the beam current would decrease slightly. As mentioned in the Apparatus and Procedure, the discharge current was increased to maintain a constant beam current. Thus, as the total voltage was decreased, the E_I had to be increased to maintain a constant η_u. This effect is shown in Fig. 14. At a beam current of 1.5 A, the total voltage was lowered from 1600 to 1400 volts at a constant R. At an η_u of 86 percent E_I increased by about 25. This degradation was probably the result of the plasma sheath at the screen grid moving away from the discharge chamber as the total voltage was lowered and creating a smaller effective grid open area.[13]

Direction of grid dish. - Figure 15 is a plot of E_I versus η_u for tests 2 and 3 of Table II where the cold grid spacings were identical but the dish directions were opposite. The data were obtained at a beam current of 2.0 amperes. The total accelerating voltages necessary to operate about 200 volts above the knee were 1350 and 1800 volts for tests 2 and 3, respectively.

As shown previously, operation at a lower total voltage degraded discharge chamber performance. However, it is shown in Fig. 15 that at an E_I of 350, the η_u of test 2 was 12 percent higher than test 3. This occurred even though test 2 was operated at a total voltage 450 volts less than test 3. This effect was probably due to the decreased hot spacing for the convex grids of test 2 and the increased hot spacing for the concave grids of test 3. Reference 13 has also shown that E_I increased as the grid spacing was increased.

Thrust Losses

Thrust Losses from Hole Misalinement

The losses in thrust, calculated from Eqs. (14) and (15) arising from grid hole misalinement due to the separation of dished grid are presented in Fig. 16. Figure 16 shows the normalized thrust to beam power ratio plotted as a function of grid dish depth for a 30-cm diameter thruster. As explained in Ref. 11, the thrust loss is a function of the ratio of the cold grid spacing to hole diameter ratio ℓ_g/D_S. Therefore, two values of ℓ_g/D_S, similar to those used experimentally, are shown. The case of no misalinement is also shown. In this case, the grids are assumed to be fabricated in such a fashion as to allow the ions to be ejected normal to the grid surface and the thrust loss is due only to the spherical shape of the grid surface.

For convenience it will be assumed that the actual thrust loss is midway between that predicted by use of the two different assumed ion current density profiles. Figure 16 shows that the thrust losses due to beam divergence increase with both the grid dish depth and the ℓ_g/D_S ratio. The divergence loss for the case of no misalinement varies from about 0.5 to 5 percent as the dish depth increases from 1.27 to 3.81 cm. For the case of misalined grid holes, the thrust loss increases strongly with the ℓ_g/D_S ratio.

A dish depth of 2.54 cm and ℓ_g/D_S ratios of 0.23 and 0.6 were used for the experimental data of this paper. For these grid geometries the estimated thrust losses were between 4 and 8 percent.

Methods of Reducing Thrust Losses

The inherent thrust losses of present dished grids can be reduced if the geometry of the dished grids is such that the hole misalinement is lessened or even misalined such that the beamlet deflection, λ, corrects for the angle γ.

Two techniques which may help reduce or change the sign of λ are hole pattern compensation and/or dishing with a spacer between the screen and accelerator grid. Hole pattern compensation corrects the misalinement by using a different hole center-to-center spacing for the screen grid than for the accelerator grid. For grids dished concave the screen grid hole center-to-center spacing would be greater than that of the accelerator. For grids dished convex, the screen grid hole center-to-center spacing would be less than that of the accelerator grid. Grids fabricated with these two slightly different center-to-center spacings would be hydroformed in the normal simultaneous manner. The angle λ could also be reduced by dishing the grids with a hydroformable spacer sheet between them and bonded to them. Negative values of λ could be achieved by using even thicker spacer sheets. The stress relieving would also be done with the spacer sheet in place.

Methods of Increasing the Dish Depth

The dished grid data presented in this paper is representative of approximately 50 percent open area screen grids. Substantial performance gains could be made by operation with higher open area screen grids. Attempts to hydroform higher open area grids by the technique presented earlier in this paper have resulted in rupture of the central area of the grids. Three new techniques have been tested on scale model grids and indicate ways of increasing the dish depth.

The first method of increasing the amount of dish depth tolerable for a given diameter grid is to perform a two step dishing operation. The grids would be hydroformed to near their rupture limit, then stress relieved, and rehydroformed to a dish depth higher than what would be possible by a single hydroforming operation. This technique could, of course, be extended to more than two steps if necessary.

A second technique is to force the distribution of elongation of the grid to occur more uniformly over the grid face. During normal single step hydroforming into a female die, the elongation in the central area of the grid is much greater and closer to the rupture limit than near the outer edge of the grid. The elongation of the outer grid region can be forced to be larger than normal by using a two stage dishing operation. The first step consists of hydroforming the grid to a pie pan shape by using a properly shaped die. The second step simply dishes the grids to the desired contour which removes the pie pan shape and allows a deeper dish depth than the single step hydroforming.

The third technique consists of eliminating the catastrophic failure which occurs when a grid ruptures. At this point of rupture the minimum webbing areas begin to reduce in cross sectional area. This further reduces the strength of the grids in that area. As a result, the grid catastrophically ruptures (during hydroforming) in the region where the first cross sectional area reduction occurs. A method of preventing or retarding this premature rupture consists of placing a solid sheet of metal above the grids so that the grids are sandwiched between a stiff solid sheet of metal and the rubber sheet used for hydroforming. Local weak areas caused by hole irregularities in the grids are then no longer sites of premature rupture since they are strengthened by the resistance of hydroforming the stiff solid sheet.

These three hydroforming technique variations are entirely independent; thus any or all could be used for increasing the amount of dish depth.

Two additional but yet untested techniques to obtain a deeper dish would hydroform the molybdenum sheets prior to etching the holes. One method would simultaneously hydroform the bare blank grids, stress relieve them and then proceed with the etching process. The other method would be to deposit the photoresist on the blank grids and then hydroform them. The dished sheets would then have the holes chemically etched followed by the simultaneous stress relieving.

Lifetests

As of January 1, 1972, the set of grids used in tests 1 through 4 have accumulated 1365 hours of operation, including 700 hours at a beam current of 2.5 amperes. This set of grids has been thermally cycled in 15 separate test segments with no change in the ion extraction capability. The thruster efficiencies (not optimized for minimum fixed power losses or neutralizer flow rate) are listed in Table III. The total thruster efficiency increased from 0.60 to 0.64 and the specific impulse increased from 2620 to 2910 seconds as the beam current was increased from 1.5 to 2.5 amperes. The ideal thrust to power ratio was nearly constant at 46×10^{-6} newtons per watt (10^{-2} lbs/kw).

The familiar charge exchange ion erosion pattern on the downstream side of the accelerator was just barely visible. A plasma-bridge neutralizer, operating at 50 to 130 equivalent milliamperes, was used for these tests and did not cause any measurable grid erosion. There was a slight erosion pattern on the grid near the neutralizer but the depth was less than the surface roughness. Based on the appearance of the grids after 1365 hours, the time to erode the grids to failure should be well in excess of 10 000 hours.

Conclusions

The methods and results of the fabrication and testing of dished grids on a 30-cm diameter thruster have been presented. It was found necessary that the screen and accelerator be simultaneously hydroformed and then simultaneously stress relieved to provide matched contours of the two grids. Thus when separated, the spacing was uniform over the entire grid surface. When heated to operating temperature, the dished design permitted a controlled thermal expansion of the grids which resulted in repeatable high values of grid perveance and thrust densities. These values are equal to or greater than those of the previously tested composites and two grid accelerator systems. Ion beam currents up to 3.0 amperes have been obtained at net acceleration voltages from 500 to 1500 volts. The beam current increased as the total voltage was increased or the grid spacing was decreased but not at the powers predicted by Child's law. The accelerator system perveance and discharge chamber performance improved when a given set of dished grids was mounted convex, as viewed from downstream of the thruster.

One of the grid sets tested has accumulated 1365 hours of operation, 700 of which have been at a beam current of 2.5 amperes. There has been no significant erosion problems with the grids to date.

From these preliminary results, a closely-spaced, dished accelerator grid system appears to be a solution to the stringent requirements imposed by the near term, high thrust, low specific impulse electric propulsion missions.

Appendix - Symbols

A_o screen grid open area, cm^2

C a constant

D_s screen grid hole diameter, cm

dA elemental screen grid area, cm^2

E_I discharge energy per beam ion, eV/ion

h grid dish depth, cm

J_B ion beam current, ampere

j beam current density, amp/cm^2

ℓ ion acceleration distance, grid spacing plus screen grid thickness, cm

ℓ_g grid-to-grid spacing, cm

$\Delta\ell$ change in ion acceleration distance, cm

m/q charge to mass ratio, 0.4811×10^6 coulomb/kg for Hg^+

P_B ion beam power, kW

R ratio of net to total ion accelerating voltage

R_g radius of curvature of dished grid, cm

R_r radius of grid mounting ring or half chord length of dished grid, cm

r radial distance from beam axis to any point on grid, cm

S arc length of dished grid, cm

T thrust of ion engine, newton

ΔT_g mean temperature increase of grid, ^oC

ΔT_r mean temperature increase of mounting ring, ^oC

ΔV knee value of total accelerating voltage, volts

v ion velocity, m/sec

Δz change center of curvature of grid before and during operation, cm

α coefficient of thermal expansion, $^oC^{-1}$

β angle between hot and cold radii of curvature at some point on grid, radians

γ angle between thruster axis and any point on grid, radians

γ_{max} maximum angle of dish, radians

ϵ_o permittivity of free space 8.85×10^6 $coulomb^2$/newton-meter

η_u propellant utilization efficiency

θ aximuthal angle defining position of r, radians

λ beam deflection angle due to grid hole misalinement, radians

Superscript:

' prime denoting grid dimensions at room temperature prior to operation

Subscripts:

A accelerator grid

S screen grid

References

1. Bartz, D. R., and Horsewood, J. L., "Characteristics, Capabilities, and Costs of Solar Electric Spacecraft for Planetary Missions," Journal of Spacecraft and Rockets, Vol. 7, No. 12, Dec. 1970, pp. 1379-1390.

2. Strack, W. C., and Hrach, F. J., "Early Application of Solar-Electric Propulsion of a 1-Astronomical-Unit Out-of-the Ecliptic Mission," TN D-5996, 1970, NASA, Cleveland, Ohio.

3. Bechtel, R. T., "Performance and Control of a 30-Cm-Diam, Low-Impulse, Kaufman Thruster, Journal of Spacecraft and Rockets, Vol. 7, No. 1, Jan. 1970, pp. 21-25.

4. Bechtel, R. T., "Component Testing of a 30-Centimeter Diameter Electron Bombardment Thruster," Paper 70-1100, Sept. 1970, AIAA, New York, N.Y.

5. King, H. J. and Poeschel, R. L., "Low Specific Impulse Ion Engine," NASA CR-72677, Feb. 1970, Hughes Research Labs., Malibu, Calif.

6. Bechtel, R. T., Banks, B. A., and Reynolds, T. W., "Effect of Facility Backsputtered Material on Performance of Glass-Coated Accelerator Grids for Kaufman Thrusters," Paper 71-156, Jan. 1971, AIAA, New York, N.Y.

7. Pawlik, E. V., Macie, T., and Ferrera, J., "Electric Propulsion System Performance Evaluation," Paper 69-236, Mar. 1969, AIAA, New York, N.Y.

8. Kerslake, W. R., and Pawlik, E. V., "Additional Studies of Screen and Accelerator Grids for Electric-Bombardment Ion Thrustors," TN D-1411, 1963, NASA, Cleveland, Ohio.

9. Finke, R. C., Holmes, A. D., and Keller, T. A., "Space Environment Facility for Electric Propulsion Systems Research," TN D-2774, 1965, NASA, Cleveland, Ohio.

10. Kerslake, W. R., "Accelerator Grid Tests on an Electric-Bombardment Ion Rocket," TN D-1168 1962, NASA, Cleveland, Ohio.

11. Lathem, W. C., and Adam, W. B., "Theoretical Analysis of a Grid-Translation Beam Deflection System for a 30-cm Diameter Kaufman Thruster," TM X-67911, 1971, NASA, Cleveland, Ohio.

12. Kerslake, W. R., "Charge-Exchange Effects on the Accelerator Impingement of an Electron-Bombardment Ion Rocket," TN D-1657, 1963, NASA, Cleveland, Ohio.

13. Byers, D. C., "An Experimental Investigation of a High-Voltage Electron-Bombardment Ion Thruster," Journal of the Electrochemical Society, Vol. 116, No. 1, Jan. 1969, pp. 9-17.

14. Bechtel, R. T., "Discharge Chamber Optimization of the SERT II Thruster," Journal of Spacecraft and Rockets, Vol. 5, No. 7, July 1968, pp. 795-800.

TABLE I. - DISHED GRID GEOMETRIES

Grid set	Grid	Etch	Minimum hole diameter,	Equivalent percent open area	Maximum hole diameter (on upstream surface), mm	Equivalent percent open area	Hole center-to-center spacing, mm
A	screen	50-50	1.9	51.0	2.0	58.0	2.54
	accelerator	50-50	1.9	51.0	2.0	58.0	
B	screen	90-10	1.9	51.0	2.3	73.4	2.54
	accelerator	50-50	1.9	51.0	2.0	58.0	
C	screen	50-50	1.2	48.5	1.4	58.9	1.71
	accelerator	90-10	1.2	48.5	1.5	70.3	

Sketch of etches

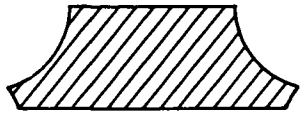

90-10

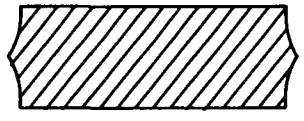

50-50

TABLE II. - GRID SPACING AND PERFORMANCE

Test number	Table I grid design	Dish direction	Cold grid spacing, mm	Estimated ion acceleration distance mm	Knee voltage for beam current of:					
					0.7 A	1.0 A	1.5 A	2.0 A	2.5 A	3.0 A
1	A	convex	0.66	0.78	630 V	720 V	830 V	1010 V	1090 V	----
2	A	convex	0.86	0.98	740	------	980	1140	1260	1420
3	A	concave	0.86	1.50	920	1040	1290	1550	------	----
4	A	concave	0.33	0.97	720	850	980	1160	------	----
5	B	convex	0.86	0.98	740	840	980	1140	1260	1420
6	C	concave	0.30	0.94	820	960	1220	1330	1500	----

TABLE III. - LIFETEST PERFORMANCE

Total hours at beam current below	25	375	200	700
Table II test number for data below	2	2	1	1
Beam current, amps	0.7	1.5	2.0	2.5
Net accelerating voltage, volts	800	900	1000	1000
Accelerator current, amps	0.0015	0.004	0.006	0.008
Accelerator voltage, volts	400	450	500	500
Emission current, amps	6.0	13.8	20.0	25.0
Discharge voltage, volts	40	40	40	40
Fixed power loss, watts	87	92	98	103
Total input power, watts	890	2000	2907	3615
Power efficiency, η_p	0.63	0.68	0.69	0.69
Utilization efficiency, η_u	0.73	0.88	0.90	0.93
Total efficiency, η_T	0.46	0.60	0.62	0.64
Specific impulse, sec	2520	2620	2820	2910
Ideal thrust Newton (mlb.)	0.041 (9.2)	0.093 (21)	0.131 (58)	0.164 (73)
Ideal thrust to power ratio N/w$\times 10^6$	46	46	45	45

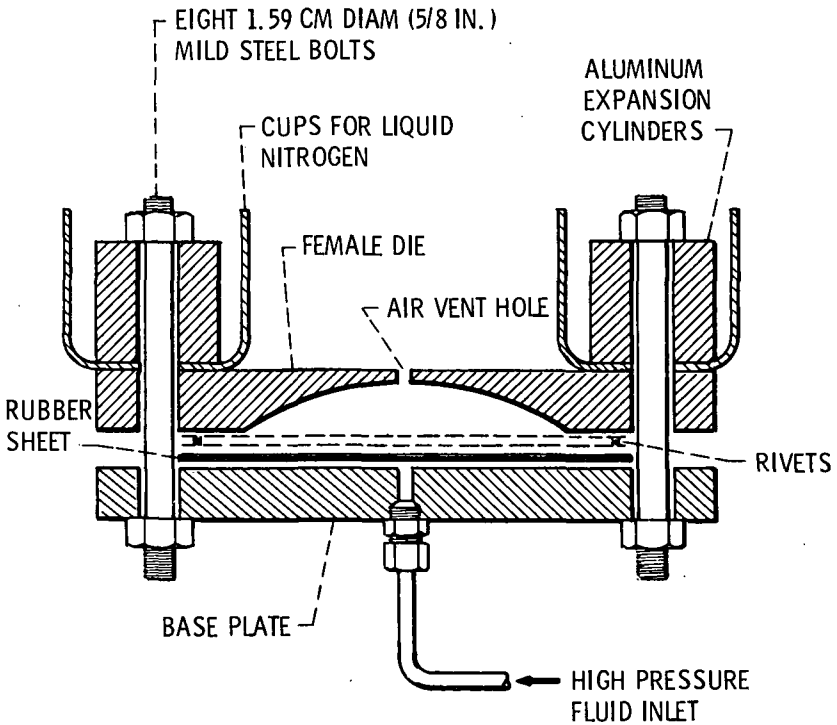

Figure 1. - Hydroforming apparatus.

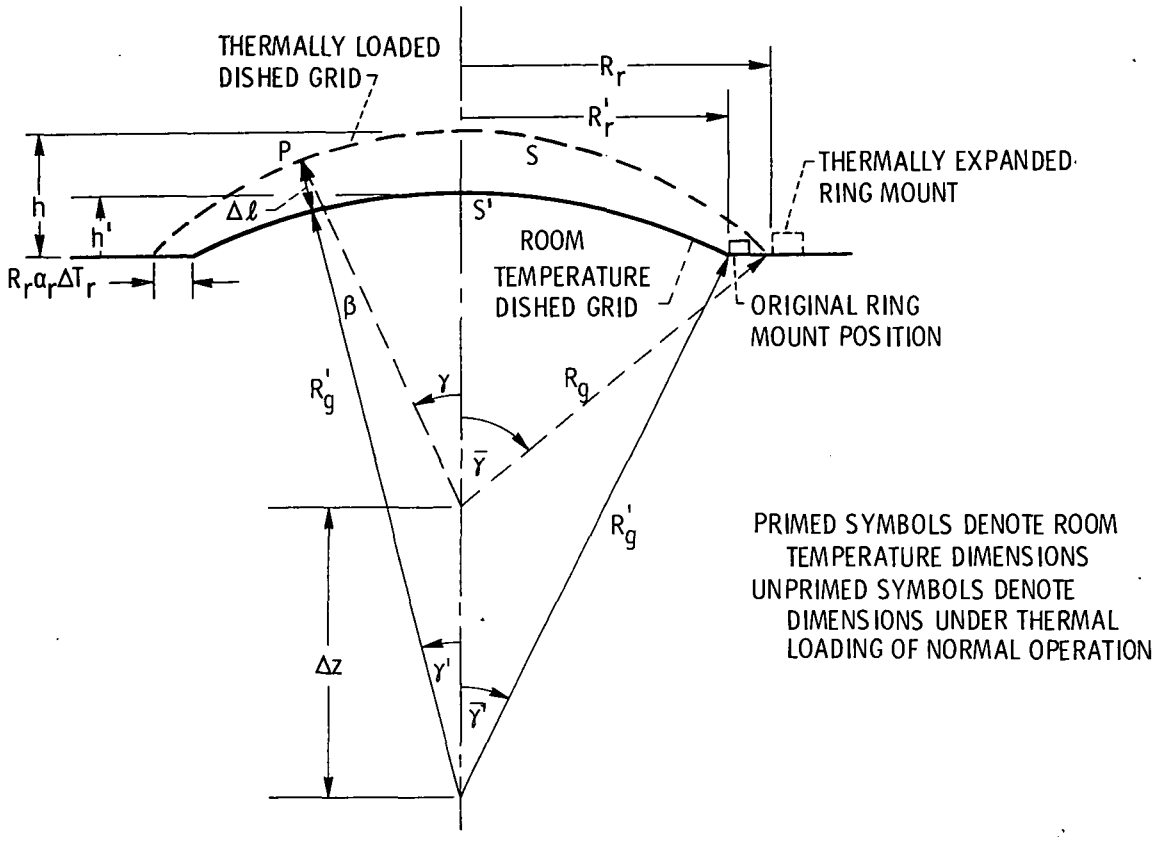

Figure 2. - Model used for grid deflection calculations.

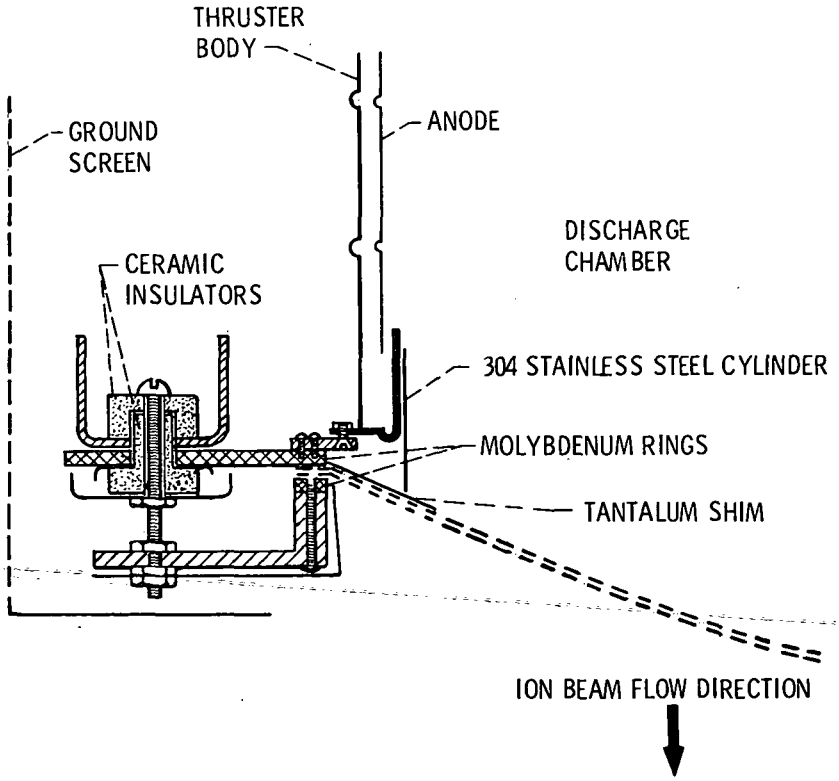

Figure 3. - Mounting system for grids dished convex.

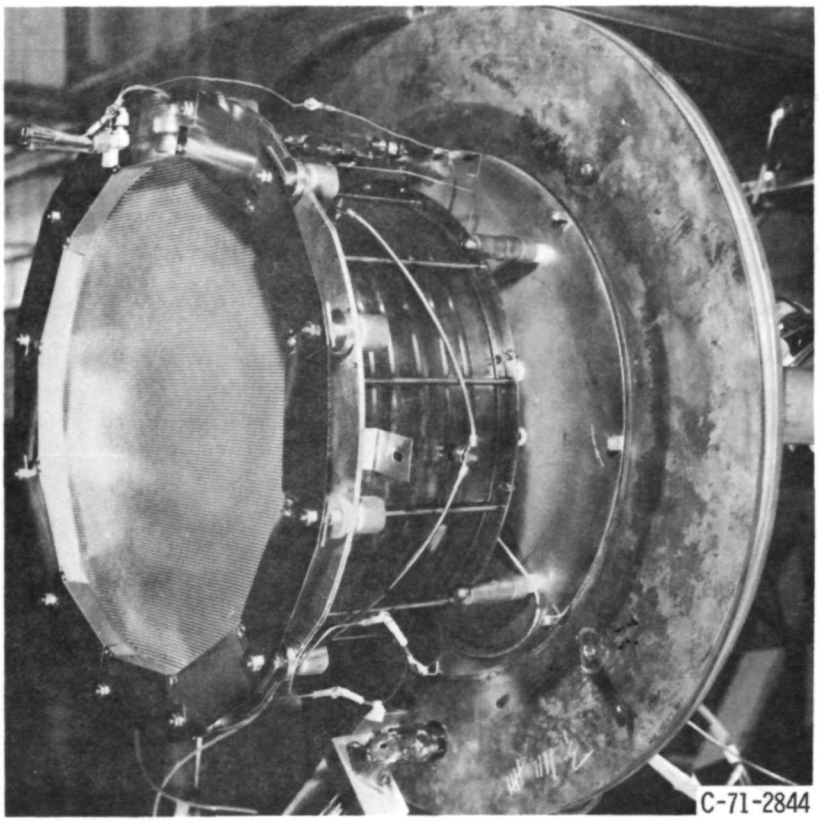

Figure 4. - Dished grid mounted concave on thruster.

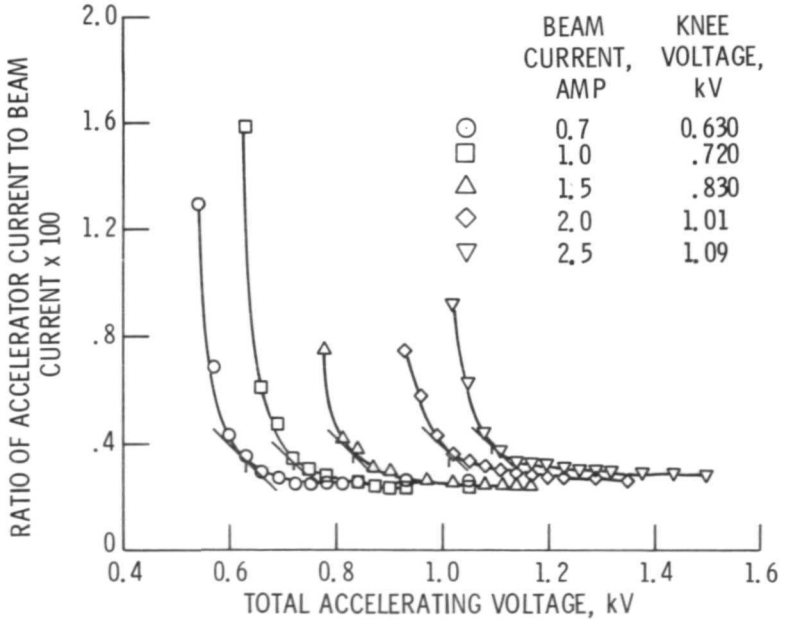

Figure 5. - Determination of minimum or knee voltage for various beam currents for grids of test 1, R = 0.67.

E-6796

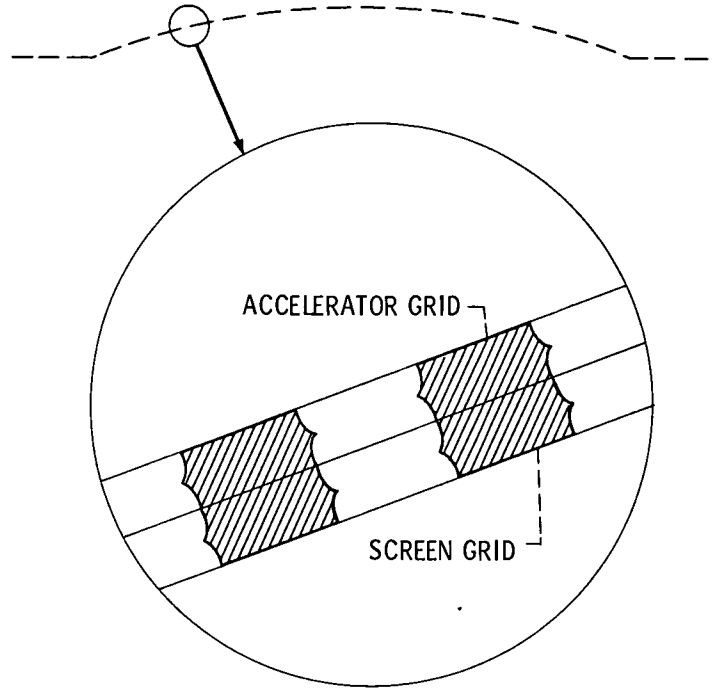

(a) AFTER HYDROFORMING AND STRESS RELIEVING.

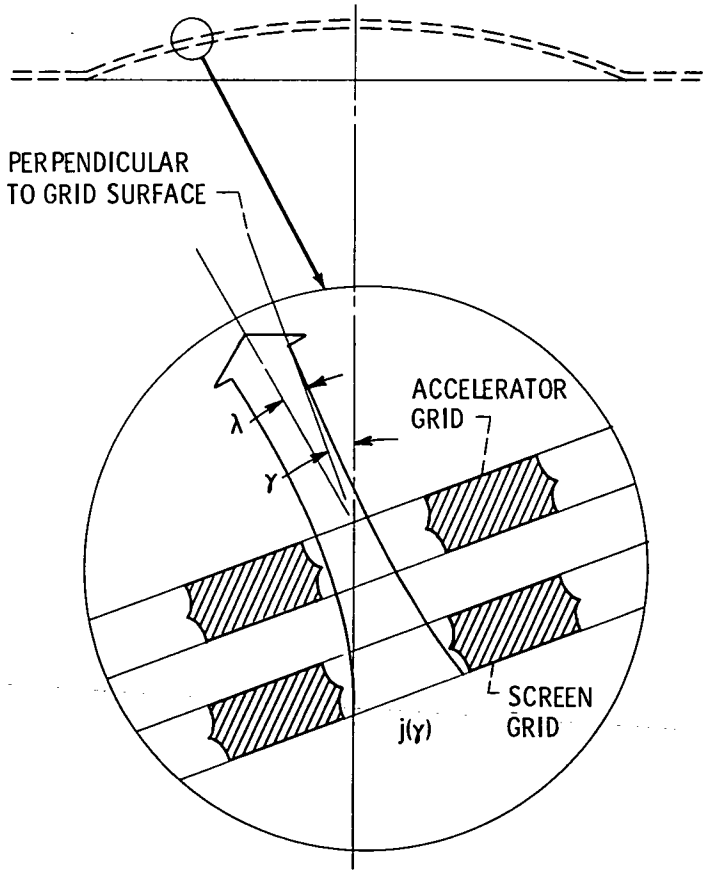

(b) AFTER SETTING GRID SPACING AND DURING OPERATION.

Figure 6. - Section views of dished grids.

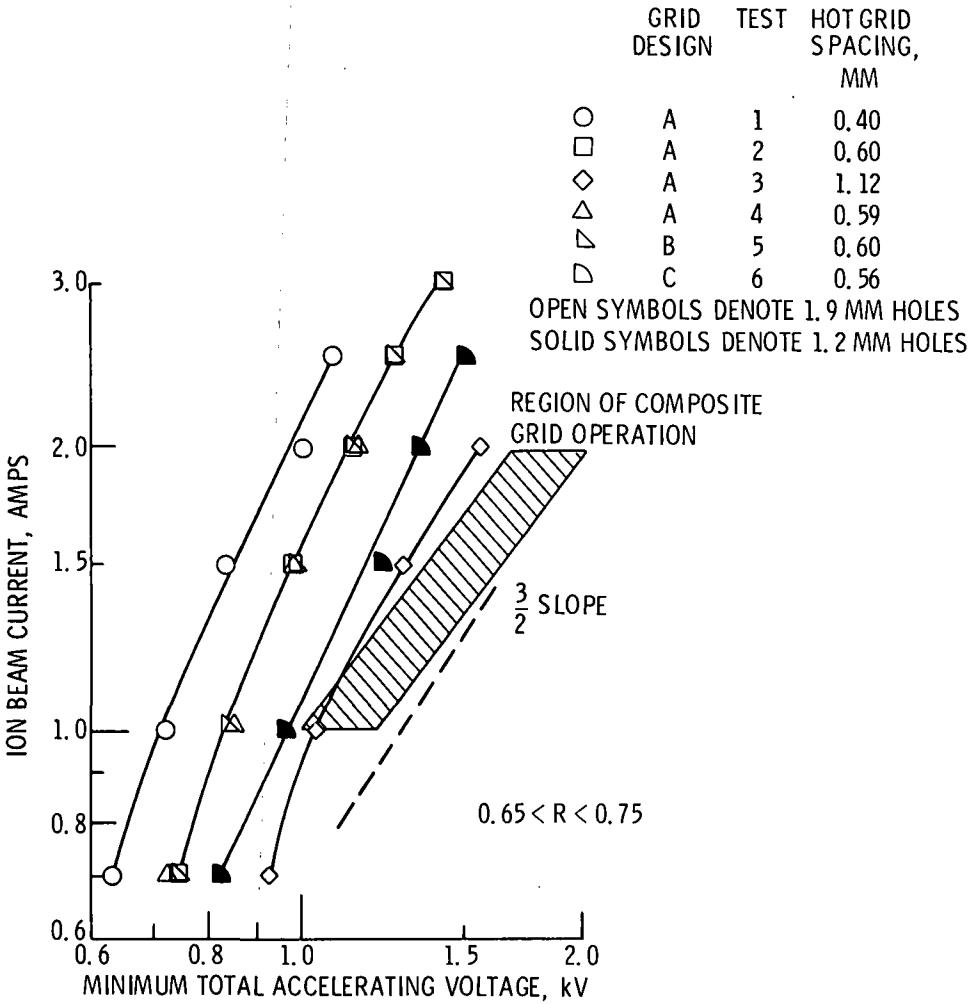

Figure 7. - Ion beam current as a function of minimum total accelerating voltage for grid sets of Table II.

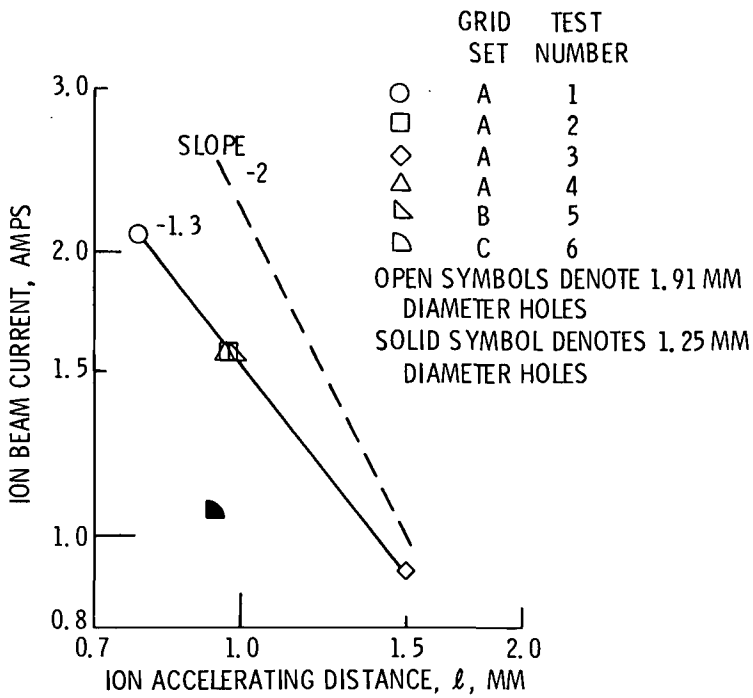

Figure 8. - Ion beam current as a function of estimated hot spacing for several grid sets at a total voltage of 1 kV.

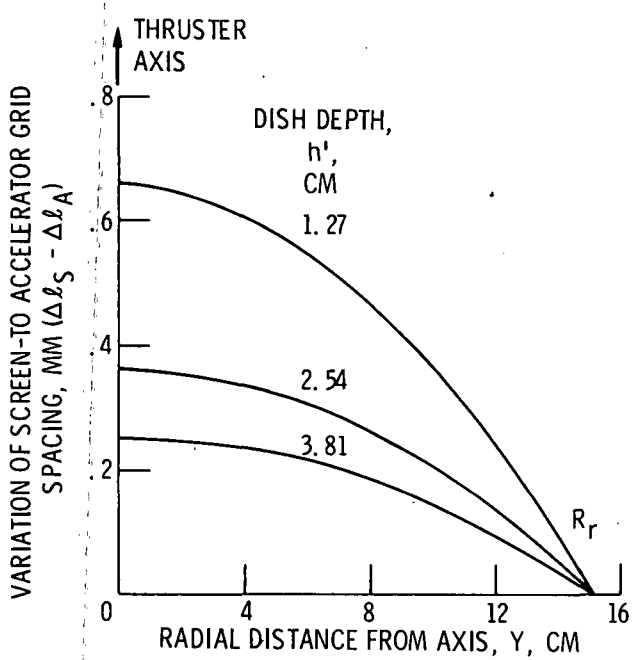

Figure 9. - Screen-to-accelerator grid spacing variation during operation R'_r, 15 cm; ΔT_{gS} = 400 C, ΔT_{gA} = 300 C.

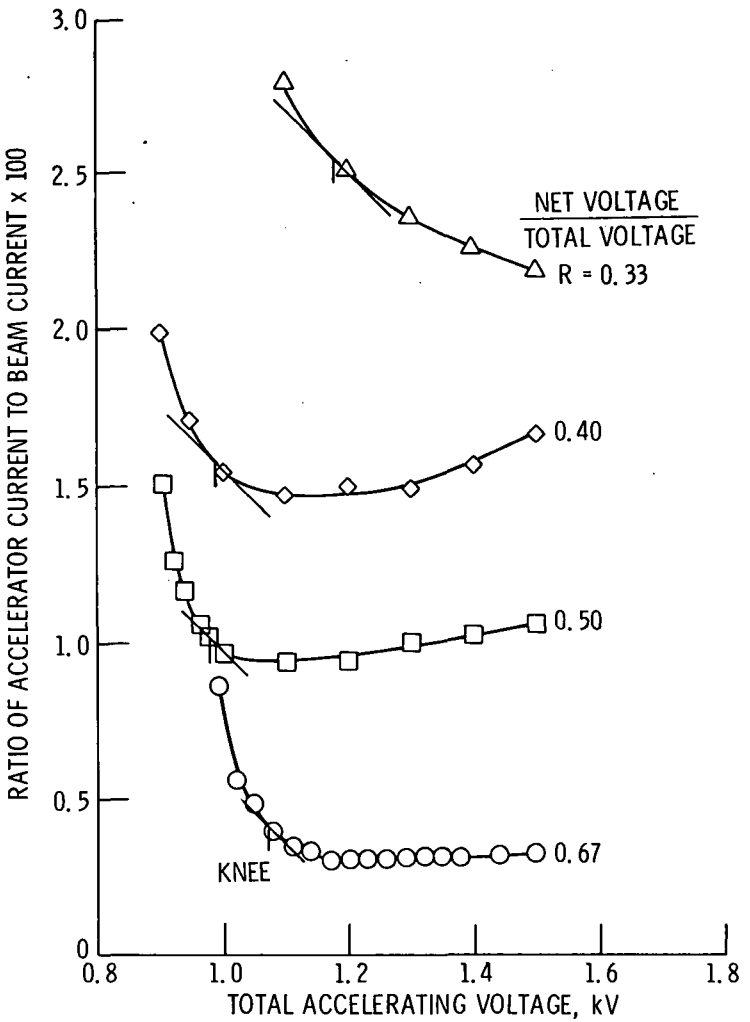

Figure 10. - Ratio of accelerator current to beam current as a function of the total accelerating voltage for several values of R. (Test 2, Table II.)

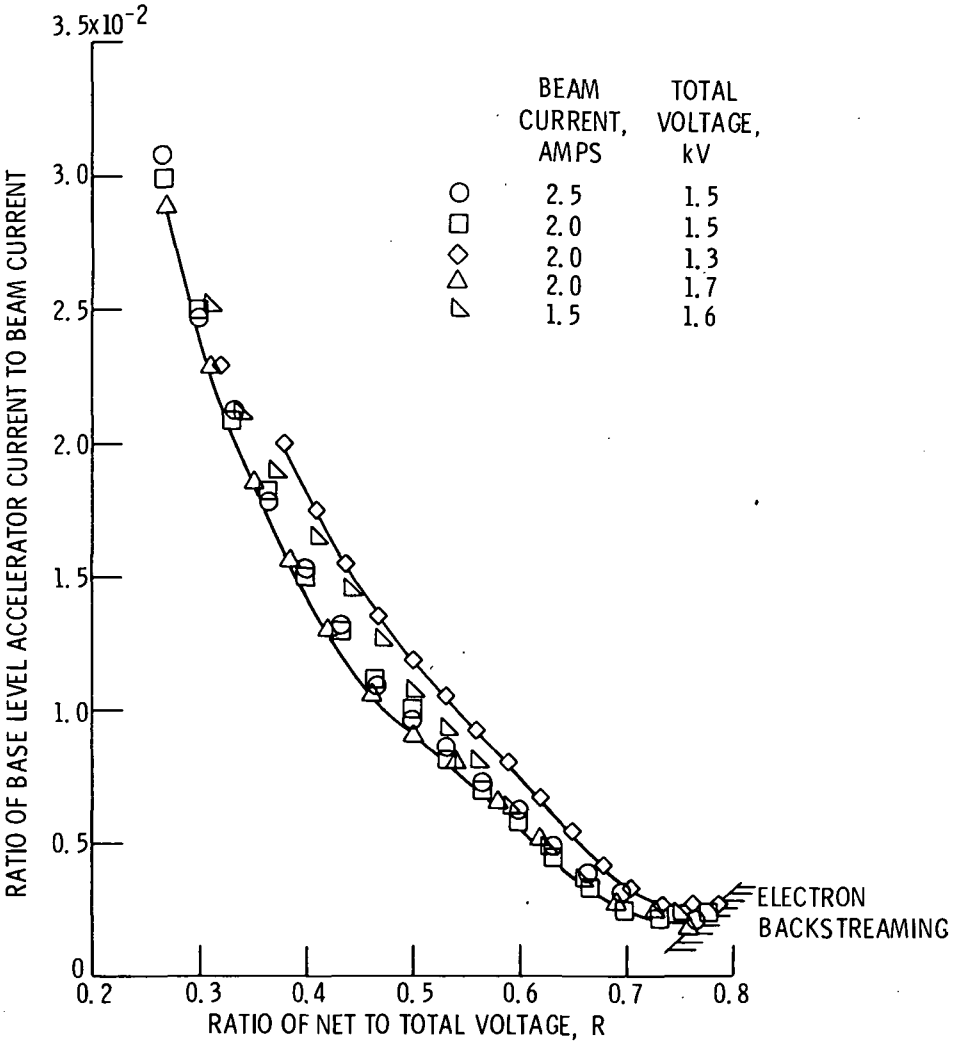

Figure 11. - Base level ratio of accelerator current to beam current as a function of net-to-total voltage ratio for several beam currents and total voltages. (Test 2, Table II) $\eta u > 0.85$.

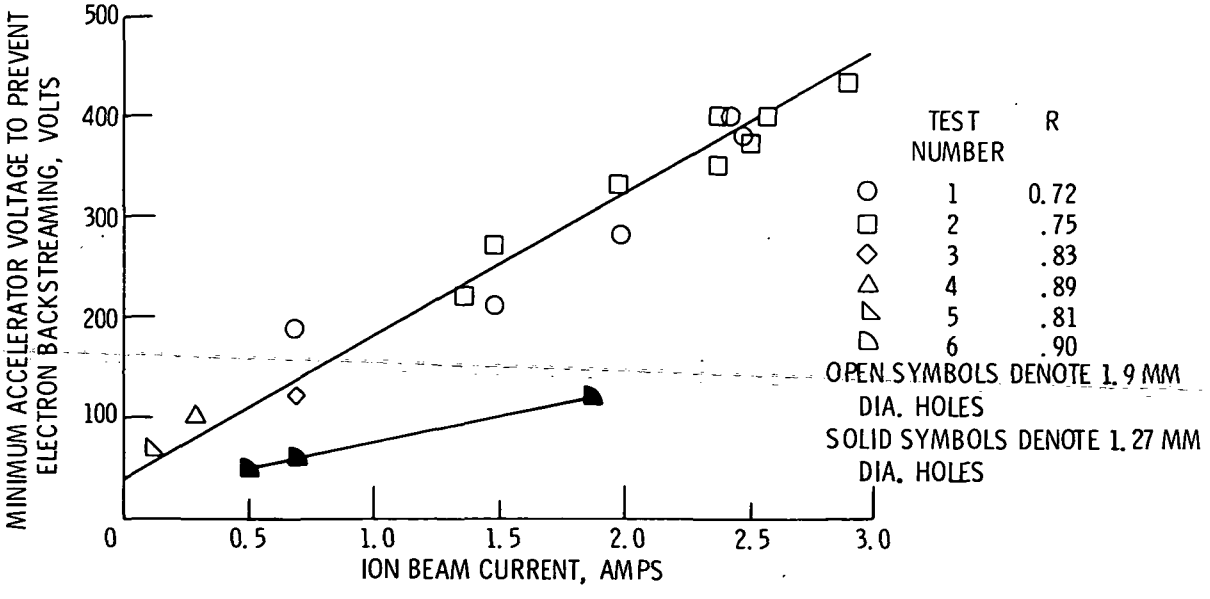

Figure 12. - Electron backstreaming limit of accelerator voltage as a function of beam current for several grid sets.

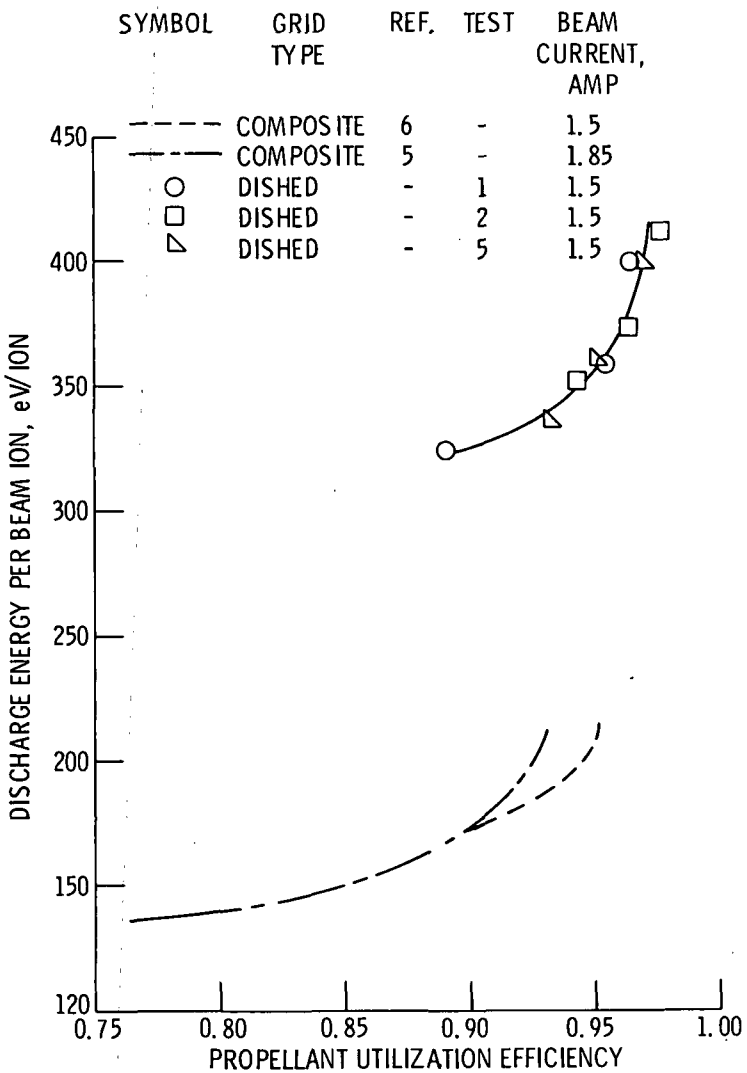

Figure 13. - Discharge chamber performance with composite grids and dished grids. (Data obtained by method 1.)

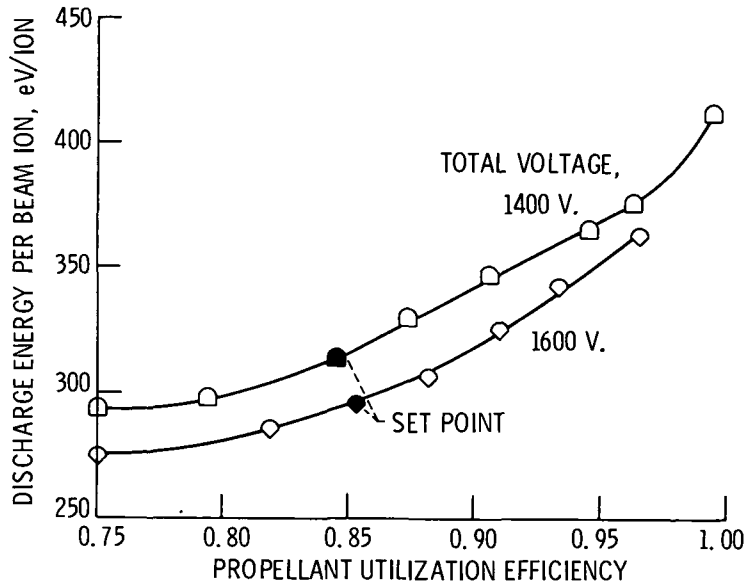

Figure 14. - Discharge chamber performance for two differeng total voltages. (Test 2, Table II)(data obtained by method 2) J_B = 1.5 amp.

E-6796

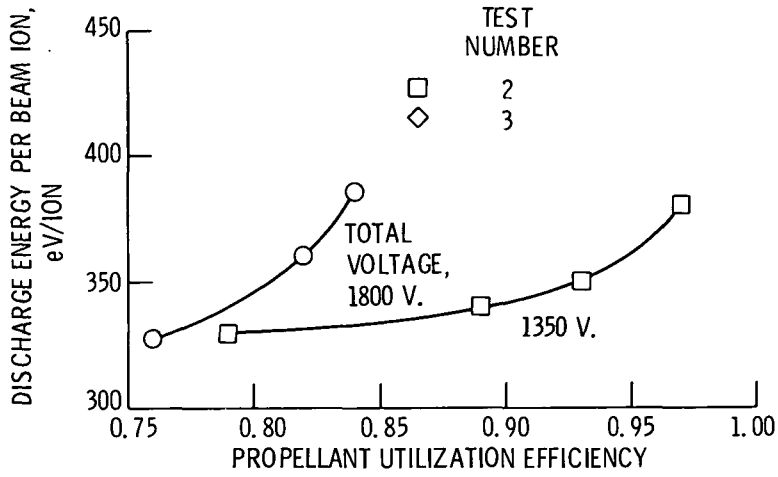

Figure 15. - Discharge chamber performance for grids with same cold spacing and different dish directions. (Data obtained by method 1) J_B = 2.0 amp.

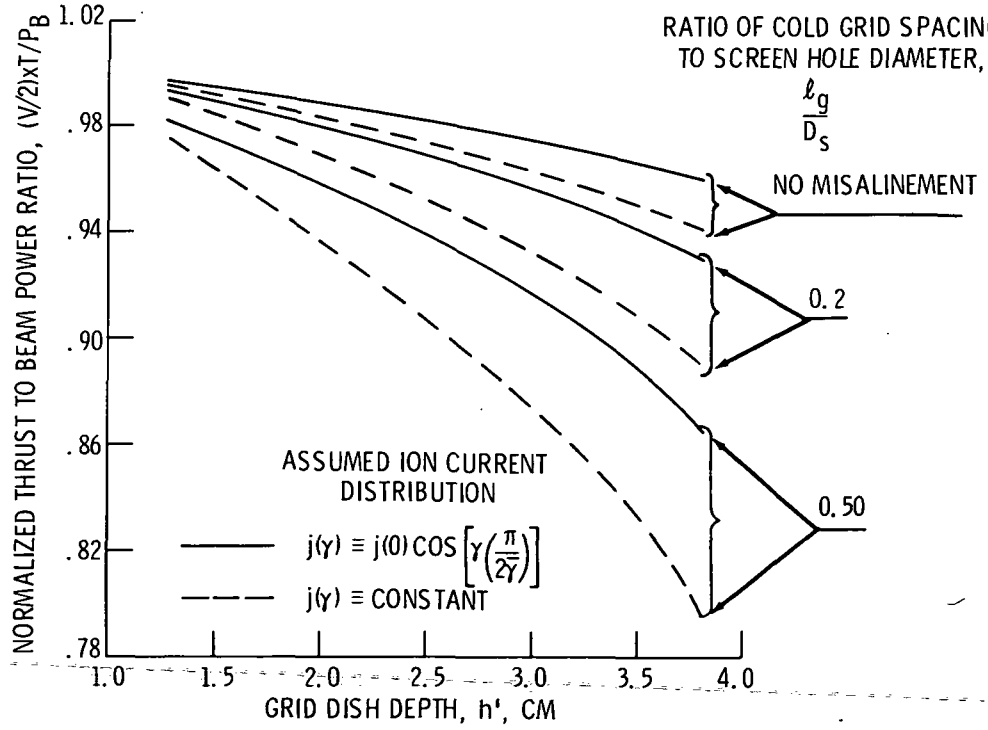

Figure 16. - Ratio of thrust to beam power as a function of grid dish depth, R'_r, 15 cm.